Computational Analysis of Vortex Tube with Different Inlet Shapes

Mr. Feizal Fidus
Department of Mechanical Engineering
MA College of Engineering, Kothamangalam

Mr. Reji Mathew
Professor
Department of Mechanical Engineering
MA College of Engineering, Kothamangalam

Mr. Nidhin A R
Department of Mechanical Learning
MA College of Engineering, Kothamangalam

Mr. Swagath V Mohan
Department of Mechanical Engineering
MA College of Engineering, Kothamangalam

Mr. Jinu Chandran
Department of Mechanical Engineering
MA College of Engineering, Kothamangalam

Abstract

The vortex tube, also known as the Ranque-Hilsch vortex tube, is a mechanical device that separates a compressed gas into hot and cold streams. The air emerging from the "hot" end can reach temperatures of 200 °C, and the air emerging from the "cold end" can reach -50 °C. It has no moving parts. This study is aimed towards presenting the CFD analysis of vortex tube carried out to gain an understanding about influence of different inlet shapes on its performance are compared and analyzed while other geometrical parameters are held constant. The energy separation has been observed for five different inlet shapes and air as working fluid.

Keywords- Vortex Tube, Inlet Configuration, Temperature Separation

I. INTRODUCTION

Ranque–Hilsch vortex tube (RHVT) simply called as Vortex tube, is a device which generates simultaneously cold and hot gases using compressed gas or air as a source. The vortex tube was invented by a French physics student George Ranque by accident in 1931, while experimenting with a vortex-type pump delivering cold and hot air streams simultaneously from its ends. Ranque started a small firm exploiting commercial potential of the device he developed having no moving parts. The vortex tube slipped in However, it soon failed and the vortex tube slipped into shade until 1945 when a German physicist Rudolph Hilsch, a scientific paper on the characteristics of the vortex tube. Since then vortex tube is considered as the “Ranque Vortex Tube”, the “Hilsch Tube”, and the “Ranque–Hilsch Tube”. Because of its compactness, easy maintenance and low cost vortex tube got acceptance by industrial applications like spot cooling, cooling jackets, and chamber air cooling etc. When the a compressed gas or air inducted into the vortex tube through an inlet nozzle mostly a tangential nozzle a vortex flow is created inside the vortex called as free vortex moving towards the other end, and some portion of this leaves through the opening and other got deflected by the control valve developing a forced vortex moving at the central axis of the vortex tube and leaves the vortex tube through opposite end. Heat exchange will occur between the two streams where the free vortex looses heat and forced vortex gains heat. One outlet emerges as a hot air from the periphery of the tube farther from the inlet which termed as hot end and the other outlet emerges as a cold air from a center of the tube near the inlet which termed as cold end. This phenomenon is referred to as temperature separation effect.

II. METHODOLOGY

A. Computational Fluid Dynamics

This project is purely working on computational fluid dynamics, ie, the validation and analysis is carried out in the CFD softwares. The geometry of the vortex tube is taken from the previous journals and also the validation is done with the same. The computations are performed using the Ansys 16.2 software. Numerical computations are performed to understand the nature of flow field and the explanation for temperature separation. Steady-state Roe solver and second order upwind schemes for the continuity, momentum and energy equations are employed. To account for the turbulent flow, Reynolds stress model is used where six Reynolds averaged equations are solved at a time. Sutherland model is applied to find the viscosity of air under ideal gas conditions. Air is used as a standard working fluid where ideal gas assumption is used for modeling the compressible flow. Table 1 shows the values of the geometrical parameters of the vortex tube. Fig 1 shows the geometry of the vortex tube.

Table 1: Geometrical parameters of the vortex tube

Parameter	*Value*
Diameter of vortex tube (D)	*0.019m*
Diameter of cold end (d)	*0.007m*
Length of vortex tube (L)	*0.090m*
Semi- cone angle (α)	*25°*

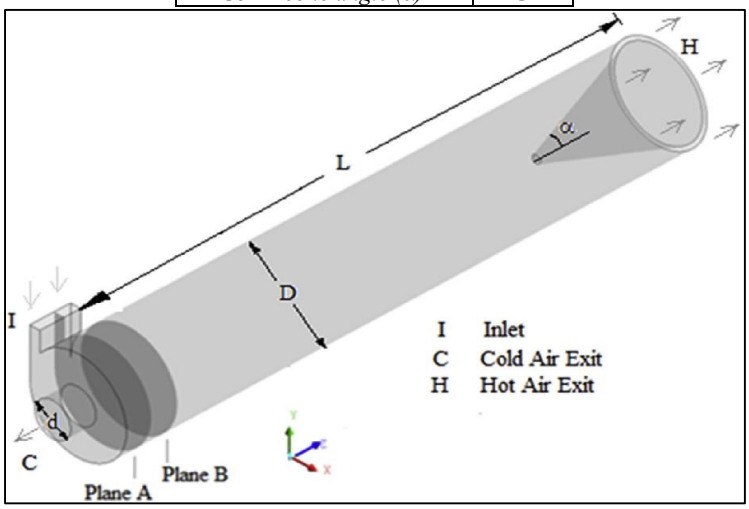

Fig. 1: Geometry of the vortex tube showing

B. Governing Equations

For the flow considered in this study, the conservation equations for mass and momentum and energy are solved.

1) Mass Conservation Equation

The equation for conservation of mass, or continuity equation, can be written as follows:

$$\frac{\partial \rho}{\partial t} + \nabla \cdot \rho \vec{v} = 0 \qquad (1)$$

where ρ is the density and $\vec{v}$ is the velocity vector.

2) Momentum conservation Equation

The conservation of momentum in an inertial (non-accelerating) reference frame is described by

$$\frac{\partial}{\partial t}(\rho \vec{v}) + \nabla \cdot (\rho \vec{v} \vec{v}) = -\nabla p + \nabla \cdot \overline{\overline{(\tau)}} + \rho \vec{g} \qquad (2)$$

where p is the static pressure, $\overline{\overline{(\tau)}}$ is the stress tensor (described below), and $\rho \vec{g}$ is the gravitational body force. The stress tensor $\overline{\overline{(\tau)}}$ is given by

$$\overline{\overline{(\tau)}} = \mu \left[\left(\nabla \vec{v} + \nabla \vec{v}^{T} \right) - \frac{2}{3} \nabla \cdot \vec{v} I \right] \qquad (3)$$

where μ is the molecular viscosity, I is the unit tensor, and the second term on the right hand side is the effect of volume dilation.

3) Energy Conservation Equation

The energy equation is solved as shown in the following form:

$$\frac{\partial}{\partial t}(\rho E) + \nabla \cdot (\vec{v} (\rho E + p)) = \nabla \cdot p + \nabla \cdot \left(k_{eff} \nabla T + \left(\overline{\overline{(\tau_{eff})}} \cdot \vec{v} \right) \right) \qquad (4)$$

where k_{eff} is the effective conductivity ($k + k_t$), where k_t is the turbulent thermal conductivity, defined according to the turbulence model being used. The first two terms on the right-hand side of Equation (4) represent energy transfer due to conduction and viscous dissipation, respectively.

$$E = h - \frac{p}{\rho} + \frac{v^2}{2} \tag{5}$$

where $h = \int_{Tref}^{T} C_p \, dT$ and T_{ref} is 298.15 K.

4) Ideal Gas Law for Compressible Flows

For compressible flows, the gas law is as following:

$$\rho = \frac{P_{op} + p}{\frac{R}{M_w} T} \tag{6}$$

where, p is the relative or gauge pressure, P_{op} is the operating pressure, M_w is the molecular weight.

5) Viscosity

Sutherland's law with three coefficients has the form

$$\mu = \mu_{ref} \left(\frac{T}{T_{ref}} \right)^{3/2} \frac{T_0 + S}{T + S} \tag{7}$$

where, μ is the viscosity in kg/m-s, T is the static temperature in K, μ_{ref} is the reference viscosity in kg/m-s, T_{ref} is the reference temperature in K, S is the sutherland constant, an effective temperature in K.

For air at specified temperatures and pressures, μ_{ref} =1.716× 10^{-5} kg/m-s, T_{ref}= 273.11 K, and S =110.56 K.

6) Turbulence Modeling

The exact transport equations for the transport of the Reynolds stresses, $\rho\overline{u_i' u_j'}$, is written as follows:

$$\frac{\partial}{\partial t}\left(\rho\overline{u_i' u_j'}\right) + \frac{\partial}{\partial x_i}\left(\rho u_k \overline{u_i' u_j'}\right) = -D_{T,ij} + D_{L,ij} - P_{ij} - G_{ij} + \varphi_{ij} - E_{ij} - F_{ij} \tag{8}$$

where, $D_{T,ij}$ refers to turbulent diffusion, $D_{L,ij}$ refers to molecular diffusion, P_{ij} refers to stress production, G_{ij} refers to buoyancy production, φ_{ij} refers to pressure strain, E_{ij} refers to dissipation, F_{ij} refers to production by system rotation.

$$D_{Ti,j} = \frac{\partial}{\partial x_k}\left(\frac{\mu_t}{\sigma_k}\frac{\overline{\partial u_i' u_j'}}{\partial x_k}\right) \tag{9}$$

$$D_{Li,j} = \frac{\partial}{\partial x_k}\left(\mu \frac{\partial}{\partial x_k}\left(\overline{u_i' u_j'}\right)\right) \tag{10}$$

$$P_{i,j} = \rho\left(\overline{u_i' u_k'}\frac{\partial u_j}{\partial x_k} + \overline{u_j' u_k'}\frac{\partial u_i}{\partial x_k}\right) \tag{11}$$

$$G_{i,j} = \frac{\mu_t}{\rho\, Pr_t}\left(g_i \frac{\partial T}{\partial x_j} + g_j \frac{\partial T}{\partial x_i}\right) \tag{12}$$

g_i is the component of gravitational acceleration vector in ith direction

$$\varphi_{i,j} = \overline{p\left(\frac{\partial u_i'}{\partial x_j} + \frac{\partial u_j'}{\partial x_i}\right)} \tag{13}$$

$$E_{i,j} = 2\mu\left(\frac{\overline{\partial u_i'}}{\partial x_k}\frac{\partial u_j'}{\partial x_k}\right) \tag{14}$$

$$F_{i,j} = -2\rho\Omega_k\left(\overline{u_j' u_m'}\varepsilon_{ikm} + \overline{u_j' u_m'}\varepsilon_{jkm}\right) \tag{15}$$

In general, when the turbulence kinetic energy is needed for modeling a specific term, it is obtained by taking the trace of the Reynolds stress tensor:

$$k = \frac{1}{2}\overline{u_i' u_i'} \tag{16}$$

A transport equation is solved for the turbulence kinetic energy in order to obtain boundary conditions for the Reynolds stresses. In this case, the following model equation is used:

$$\frac{\partial}{\partial t}(\rho k) + \frac{\partial}{\partial x_i}(\rho k u_i) = \frac{\partial}{\partial x_j}\left[\left(\mu + \frac{\mu_t}{\sigma_\varepsilon}\right)\frac{\partial k}{\partial x_j}\right] + \frac{1}{2}[P_{ii} + G_{ii}] - \rho\varepsilon\left(1 + 2M_t^2\right) \tag{17}$$

where, σ_k =0.82, turbulent Mach number, $M_t = k^{0.5}/a$, a being the speed of sound.
The scalar dissipation rate, ε, is computed with a model transport equation

$$\frac{\partial}{\partial t}(\rho\varepsilon) + \frac{\partial}{\partial x_i}(\rho\varepsilon u_i) = \frac{\partial}{\partial x_j}\left[\left(\mu + \frac{\mu_t}{\sigma_\varepsilon}\right)\frac{\partial \varepsilon}{\partial x_j}\right] C_{\varepsilon 1}\frac{1}{2}[P_{ii} + C_{\varepsilon 3} G_{ii}]\frac{\varepsilon}{k} - C_{\varepsilon 2}\rho\frac{\varepsilon^2}{k} \tag{18}$$

where σ_ε = 1.0, $C_{\varepsilon 1}$ = 1.44, $C_{\varepsilon 2}$ = 1.92, $C_{\varepsilon 3}$ is evaluated as a function of the local flow direction relative to the gravitational vector.
The turbulent viscosity, μ_t , is computed as

$$\mu_t = \rho C_\mu \frac{k^2}{\varepsilon} \tag{19}$$

where Cμ = 0.09.

The RSM model requires boundary conditions for individual Reynolds stresses, $\overline{u_i' u_j'}$ and for the turbulence dissipation rate, ε. These quantities can be input directly or derived from the turbulence intensity and characteristic length.

C. Boundary Condition

The boundary conditions for all the inlet cases are maintained at an air total pressure of 5 bar (gauge) while the pressure at hot exit is 1.2 bar (gauge) and cold exit is 1 bar (gauge). The cold outlet pressure can be varied because while employing different inlet shapes, there is a tendency for reversed flow at the cold end. It is due to the fact that during experiment we are adjusting the cold and hot valves for suitable mass flow rates. But in numerical simulation, a constant mass flow rate is applicable. The data is obtained from the previous journal papers which are used for validation purposes. The inlet total temperature is maintained at 303 K as from the journal papers. The boundary conditions for the turbulent flow field terms are assigned by assuming the turbulent intensity within 5%.

D. Assumptions

The material of the vortex tube is assumed to be insulated. Thermal conductivity of the working fluid is assumed to be constant. The flow emanating from inlets for all cases are maintained constant as in the journal papers. Temperature separation refers to the total temperature difference between inlet and cold end.

E. Grid Independence Study

Table 2 shows the grid independency study results for different mesh sizes. The mesh size is considered from 0.1 million to 1.55 million number of elements. The temperature separation between inlet and cold end does not vary significantly after a mesh size of 0.7 million number of elements. Hence the mesh size of 1.5 million elements is used for further cases. Several mesh configurations such as hybrid and hexagonal types are also tested and found to yield identical temperature separation. However, the result observed from these configurations are similar to that of tetragonal mesh. Hence the tetragonal type of mesh is adopted. And also a tolerance of 0.05 mm is used in-order to reduce the skewness of the tetragonal mesh to 0.2. Due to less complexity in mesh and lower time requirements, the tetragonal mesh configuration is chosen. Fig 2 shows the mesh of the vortex tube.

Table 2: Grid independency test (inlet Rectangle, area = 6×2 mm, d_o/D = 0.37, L/D = 4.7, D = 19 mm, P_i = 5 bar, gauge)

SL NO	*ELEMENTS*	*TEMPERATURE SEPARATION (K)*
1	*100,000*	*17.3*
2	*400,000*	*20.5*
3	*700,000*	*22.07*
4	*1,500,000*	*22.1*

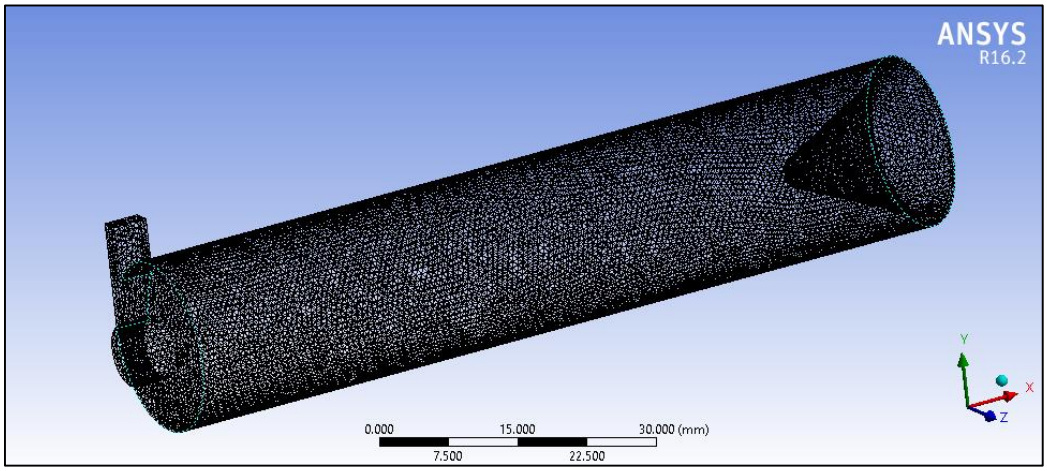

Fig. 2: Mesh of the vortex tube

III. RESULTS AND DISCUSSION

A. Validation

The validation of this project is carried out with a previous journal paper by manimaran on computational analysis of vortex tube (1). The comparison of the results is plotted in Fig3. Table 3 shows the temperature separation of the vortex tube of the present study and previous journal paper. After examining, it is found that the temperature separation of the present study is lower than the validating paper. Also there is only 9.09% variation of the results is found. To explore the effect of inlet shape and inlet angle, CFD studies are extended towards understanding the flow features and the temperature separation.

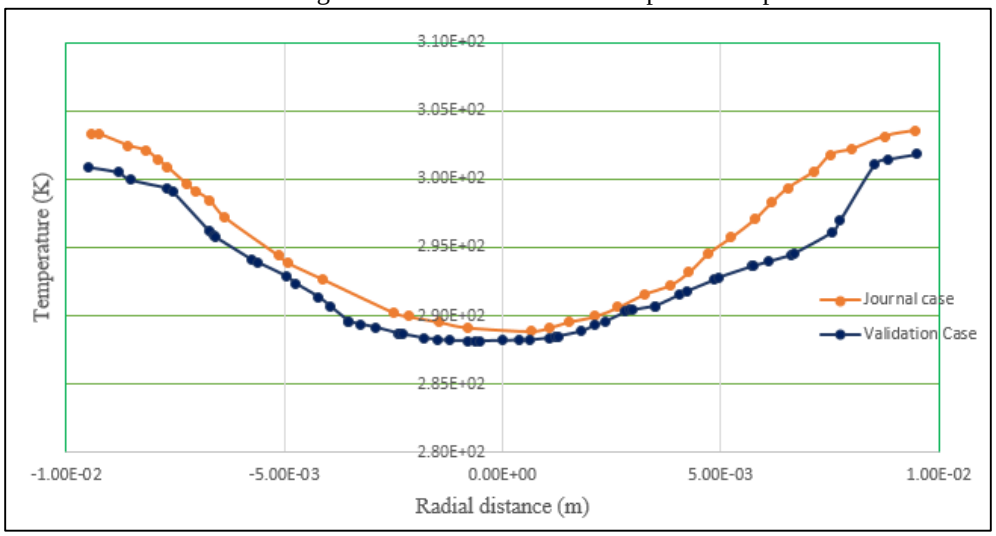

Fig. 3: Comparison of the radial distribution of Total Temperature at plane B of present study and journal case

Table 3: Table showing the percentage variation of the temperature separation between the present study and journal case (inlet Rectangle, area = 6×2 mm, dc/D = 0.37, L/D = 4.7, D = 19 mm, Pi = 5 bar, gauge)

CASE	TEMPERATURE (K)		TEMPERATURE SEPARATION (K)	% VARIATION
	MAX	MIN		
Journal	304	280	24	9.09
Validation	305	283	22	

B. Effect of Inlet Shape

In this study, five different inlet shapes are used to compare the effect of inlet shape in the performance of vortex tube. The different inlet configuration used in the study is shown in Fig 4. The cross-sectional area of every inlet configuration is maintained constant ie, area of inlet is 8 mm2. The area is held constant so that the mass flow rate for all cases remain the same, since the upstream conditions are maintained same in all cases. The same mesh is used for further simulations for all remaining cases considered.

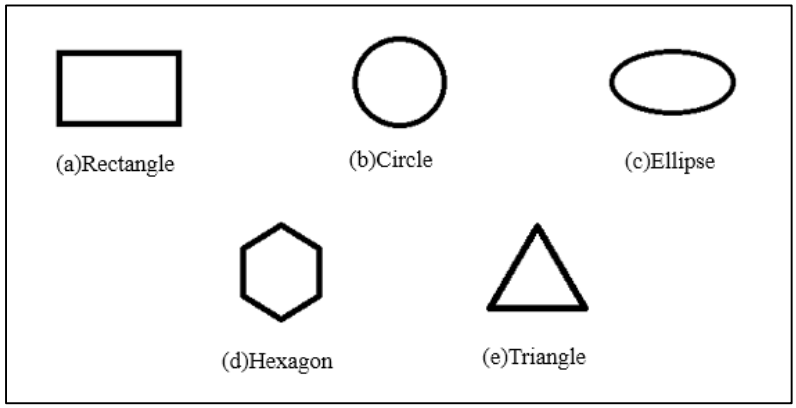

Fig. 4: Different inlet configurations used in the study

From the previous journal papers and studies, it is observed that the most of the temperature separation in the vortex tube is significant near the inlet. This is carried out by shortening the length of the vortex tube whereas the temperature separation changes a little during this transition. This conclusion is arrived as the length of the vortex tube is shortened consequently to L/D = 4.7. The energy transfer due to swirling action becomes significant near the inlet. So our study is concentrated near the inlet of the vortex tube. Due to this reason, two sections, planes A and B are chosen for discussion and comparison purposes. The physical characteristics of the vortex tube is examined along the plane B and are comparison is carried out at that location.

The radial distribution of total temperature at plane B for various inlet configurations are shown in Figure 5. The comparison indicates that the rectangular inlet shows better drop in total temperature at the core. The rectangular inlet has a temperature drop upto 276.8 K, while the circular inlet has a temperature drop of 284.9 K, which is the least. Elliptical and hexagonal inlets also shows better temperature drop of 279.7 K and 278 K respectively. Triangular inlet also has a lower temperature drop of 283.8 K. It is found that the overall trend in decrease of total temperature at the core is observed for all the inlet configurations.

Likewise the radial distribution of static temperature at plane B for different inlet configurations is plotted in Figure 6. The static temperature is found to be maximum for the rectangular inlet. Since the flow is injected into the inlet at high pressure, the flow expands after the inlet, leading to the drop in static temperature. This occurs at a radial distance of 0.008 m from the axis. Hence the lowest static temperature is found only at this location in the vortex tube. Figure 7 shows the radial distribution of static pressure at plane B for various inlet shapes. The static pressure is found to be higher at the peripheral region and decreases towards the core. The static pressure is lowest at the core region. The lowest value is about 101325 Pa. The nature of curve is similar for all cases of inlet shapes.

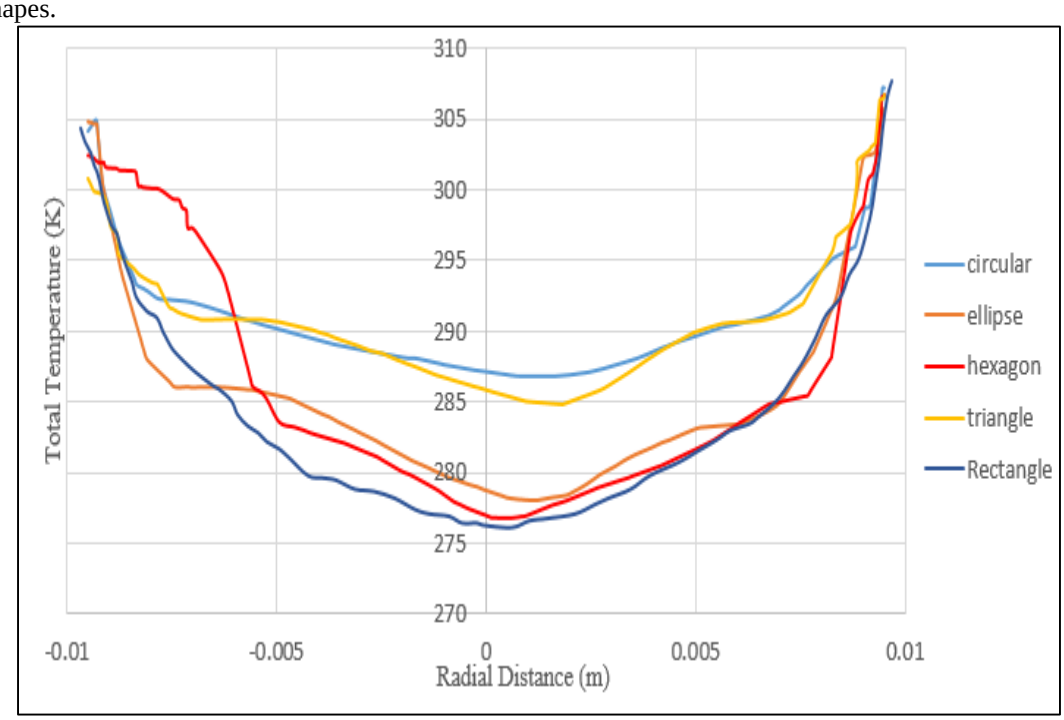

Fig. 5: Radial distribution of Total Temperature at plane B for different inlet configurations

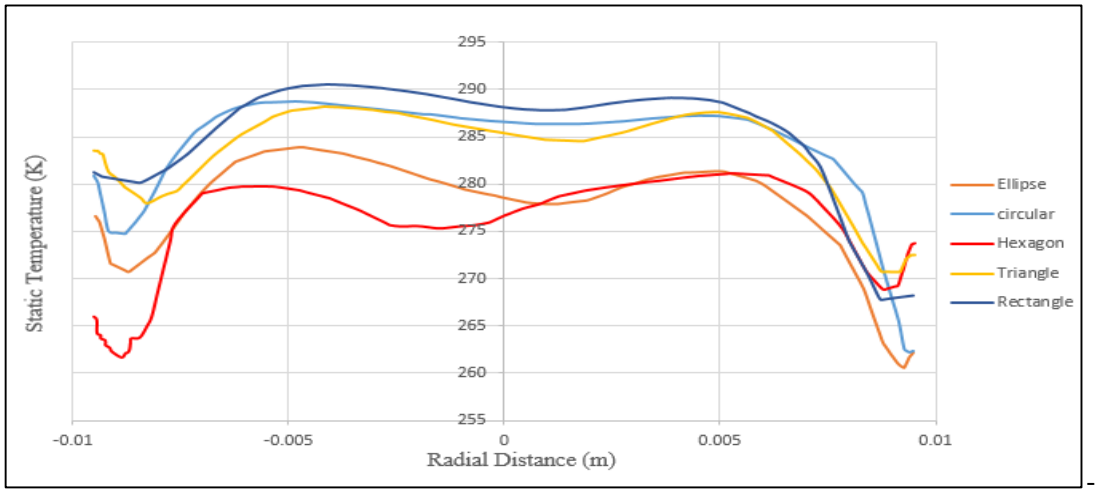

Fig. 6: Radial distribution of Static Temperature at plane B for different inlet configurations

The radial distribution of velocity magnitude at plane B for all inlet configurations is shown in figure 8. From the plot it is clear that the velocity magnitude is maximum at peripheral layers and minimum at core layers. It is because the peripheral layer fluid has swirl motion and has to travel more distance to reach the hot end and hence needs more kinetic energy, while the core layer fluid has to travel less distance to reach the cold end and needs only less kinetic energy. This is one of the reason in transferring the energy from core layer fluid to peripheral layer fluid which leads in emerging hot fluid at one end and cold fluid at another end.

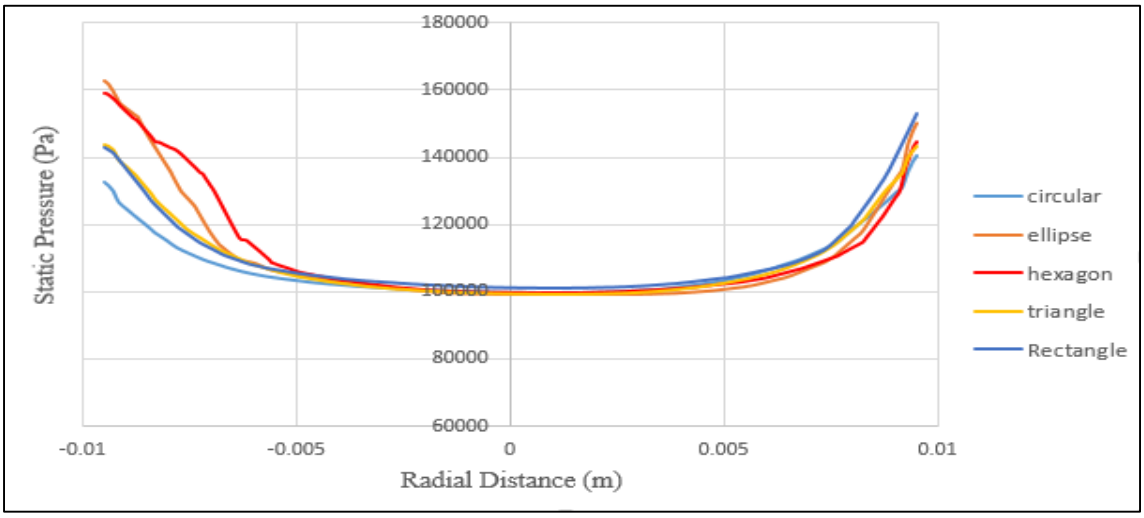

Fig. 7: Radial distribution of Static Pressure at plane B for different inlet configurations

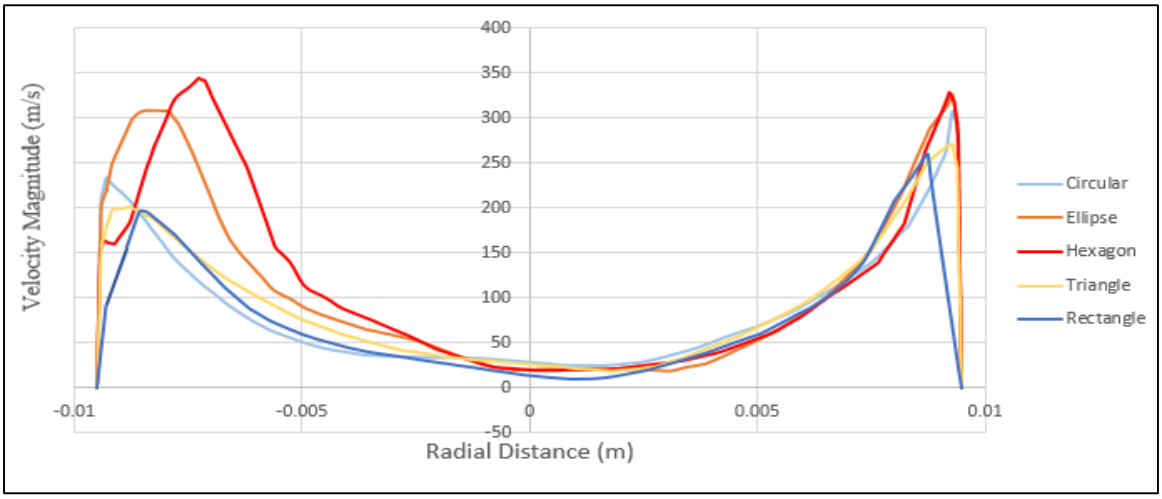

Fig. 8: Radial distribution of velocity magnitude at plane B for different inlet configurations

The axial distribution of the total temperature along the center line for all inlet configurations is shown in figure 9. From the plot, the total temperature is found to be increasing when we are moving from the inlet to the hot end. Although all inlet shapes have similar nature for the curves, rectangular inlet has better curve. It has the lower temperature value near the inlet. Elliptical and hexagonal inlet also have lower temperature similar to rectangle, but the elliptical inlet shows a rough nature in the curve. Circular and triangular inlet has much higher temperature value when compared to the others but shows a similar nature curve.

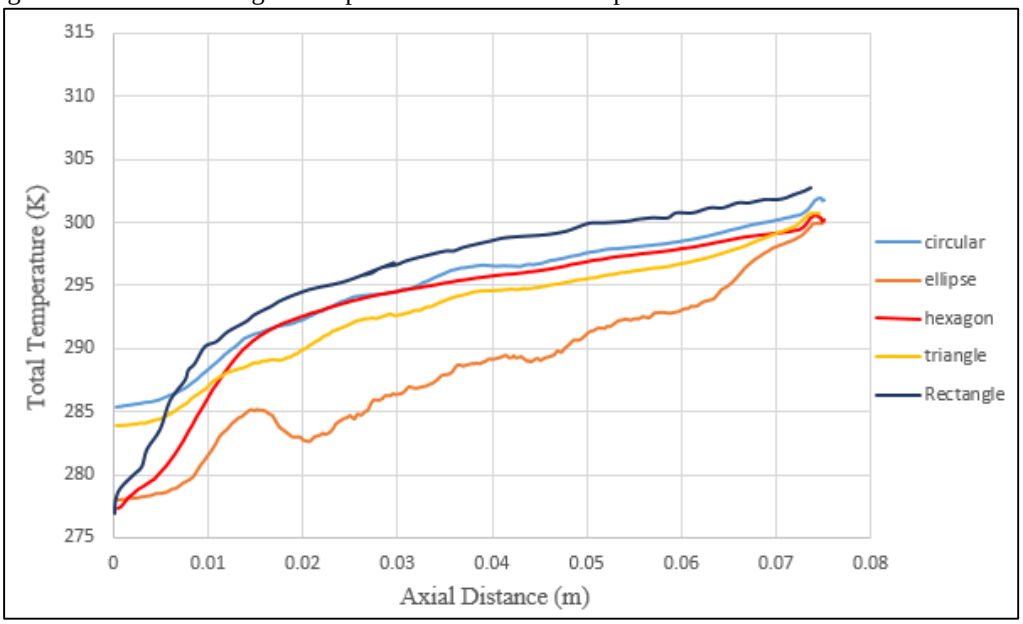

Fig. 9: Axial distribution of Total Temperature along center line for different inlet configurations

Table 4: Table showing the temperature separation and aspect ratio of various inlet configurations

SHAPES	DIMENSION		ASPECT RATIO (=W/H)	TEMPERATURE (K)		TEMPERATURE SEPARATION (K)
	WIDTH (mm)	HEIGHT (mm)		MAX	MIN	
RECTANGLE	4	2	2	305.52	276.89	26.11
CIRCLE	1.596	1.596	1	306.7	284.9	18.1
ELLIPSE	4.244	2.4	1.768	305.45	279.7	23.3
TRIANGLE	4.2983	3.7224	1.1547	306.2	283.8	19.2
HEXAGON	3.0394	1.7548	1.732	306.04	278.09	24.91

The temperature separation of all inlet configurations is shown in the Table 4. It also shows the relation of the results with the aspect ratio of the inlet shape. The inlet aspect ratio is one of the deciding parameters to determine the fluid dynamic behavior in the vortex tube. As the flow splits into peripheral and core flow at the returning point, ie, at the hot end which is farther from the inlet, it is understood that two fluid layers are formed inside the vortex tube. The thickness of peripheral flow layers and core flow layers is decided mainly by the inlet aspect ratio while the other parameters like cone shape and angle, cold end orifice diameter and length of the vortex tube are maintained constant. The inlet area is also held constant (8 mm2) in this study. The highest temperature separation between inlet and cold end is found for aspect ratio 2 which is the rectangular one with a value of 26.11 K. The lowest temperature separation is 18.1 K is found for aspect ratio 1 which is the circular inlet. From this, it is believed that inlet aspect ratio affects the performance of vortex tube significantly in such a way that inner core layers transfer their energy to outer peripheral layers. As the aspect ratio increases for all the inlet configurations, more stream lines get towards the core after the returning point from the periphery. This indicates that the energy transfer between the core and peripheral layers increases as the aspect ratio increases.

IV. CONCLUSION

The Ranque-Hilsch vortex tube is simulated with CFD data are validated with the former journal results. The performance of the vortex tube with different inlet configurations like rectangle, circle, ellipse, hexagon and triangle are studied and the compared. The study is based on several flow characteristics like total and static temperature, static pressure, velocity magnitude and temperature at the center-line of the vortex tube. The performance of the vortex tube is mainly determined from the temperature separation, ie, the temperature difference between the inlet and the cold end. Of the various inlet configurations, the rectangular inlet has the better temperature while the inlet area is held constant. It is found that, when the inlet area is held constant, the rectangular inlet has higher aspect ratio which has higher temperature separation and circular inlet has lower temperature separation which has lower aspect ratio. So the temperature separation increase with increasing aspect ratio of inlet. Hence it is concluded that the rectangular inlet has better temperature separation when the inlet area is held constant.

REFERENCES

[1] R. Manimaran, Computational analysis of energy separation in a counter-flow vortex tube based on inlet shape and aspect ratio, Energy 107 (2016) 17-28
[2] Aljuwayhel NF, Nellis GF, Klein SA (2005) Parametric and internal study of the vortex tube using a CFD model. Int J Refrig 28(3):442–450
[3] Behera U, Paul PJ, Kasthurirengan S, Karunanithi R, Ram SN, Dinesh K, Jacob S (2005) CFD analysis and experimental investigations towards optimizing the parameters of Ranque– Hilsch vortex tube. Int J Heat Mass Transf 48(10):1961–1973
[4] Bej N, Sinhamahapatra KP (2014) Exergy analysis of a hot cascade type Ranque–Hilsch vortex tube using turbulence model. Int J Refrig 45:13–24
[5] Bruun HH (1969) Experimental investigation of the energy separation in vortex tubes. J Mech Eng Sci 11(6):567–582
[6] Thakare HR, Parekh AD (2015) Computational analysis of energy separation in counter: flow vortex tube. Energy 85:62–77
[7] Dutta T, Sinhamahapatra KP, Bandyopdhyay SS (2010) Comparison of different turbulence models in predicting the temperature separation in a Ranque–Hilsch vortex tube. Int J Refrig 33(4):783–792
[8] Eiamsa-ard S, Promvonge P (2007) Numerical investigation of the thermal separation in a Ranque–Hilsch vortex tube. Int J Heat Mass Transf 50(5):821–832
[9] Farouk T, Farouk B, Gutsol A (2009) Simulation of gas species and temperature separation in the counter-flow Ranque–Hilsch vortex tube using the large eddy simulation technique. Int J Heat Mass Transf 52(13):3320–3333
[10] Fro¨hlingsdorf W, Unger H (1999) Numerical investigations of the compressible flow and the energy separation in the Ranque– Hilsch vortex tube. Int J Heat Mass Transf 42(3):415–422
[11] Hartnett JP, Eckert ERG (1957) Experimental study of the velocity and temperature distribution in a high-velocity vortextype flow. Trans ASME 79(4):751–758
[12] Kandil HA, Abdelghany ST (2015) Computational investigation of different effects on the performance of the Ranque–Hilsch vortex tube. Energy 84:207–218
[13] Khait AV, Noskov AS, Lovtsov AV, Alekhin VN (2014) Semiempirical turbulence model for numerical simulation of swirled compressible flows observed in Ranque–Hilsch vortex tube. Int J Refrig 48:132–141
[14] Skye HM, Nellis GF, Klein SA (2006) Comparison of CFD analysis to empirical data in a commercial vortex tube. Int J Refrig 29(1):71–80